Chemical Engineering Science 300 (2024) 120560

Contents lists available at ScienceDirect

Chemical Engineering Science

journal homepage: www.elsevier.com/locate/ces

Operation optimization of propane pre-cooled mixed refrigerant LNG Process: A novel integration of knowledge-based and constrained Bayesian optimization approaches

Roba Shady, Samer F. Ahmed *, Ahmad K. Sleiti

Mechanical and Industrial Engineering Department, College of Engineering, Qatar University, P O Box 2713, Doha, Qatar

ARTICLE INFO

Keywords:
Propane pre-cooled mixed refrigerant
LNG
Mixed refrigerants
Knowledge-based Optimization
Constrained Bayesian optimization
Large-scale C3MR

ABSTRACT

Liquefied natural gas (LNG) technology, particularly the propane precooled mixed refrigerant (C3MR) process, has demonstrated efficiency and emerged as a distinctive dual-refrigerant technology widely used in LNG production. However, the liquefaction process is the highest energy-intensive stage within its supply chain as it consumes about 8 % of the LNG energy content. Thus, for the first time, this study proposes systematic knowledge-based and constrained Bayesian optimization approaches to identify the optimal operation of the C3MR process. These approaches optimize both the operational parameters (pressures and flow rates) and the composition of the mixed refrigerant with practical equipment specifications and rigorous constraints. The results show that the specific energy consumption (SEC) is reduced to 0.264 kWh/kg_{LNG}, which is 14.6 %, and 26 % lower than the basic C3MR process (unoptimized case) and typical industrial C3MR processes, respectively. In addition, the optimized SEC in this study is 14.5 % to 38.6 % lower than those reported in the literature. At large-scale LNG production (10,000 tons per day), the reduction in the SEC is translated into an 18 MW decrease in compression power, saving approximately 4.7 million $ per year for each C3MR train. Moreover, the coefficient of performance (COP) of the C3MR process was improved by about 15 %, and the CO_2 emissions were reduced by 17 % (7 tons per year) compared to the basic C3MR process, indicating potential advancements in large-scale LNG liquefaction processes.

1. Introduction

As the world's population increases and economies continue to develop, there's a rapid growth in energy demand. To address this growing demand and in response to economic and environmental concerns, the demand for natural gas (NG) is expected to increase by 1.6 % per year in the upcoming decades (Xu et al., 2022). This rise is predicted to contribute to a quarter of the global energy demand by 2030 (Kumar et al., 2011; IGU World LNG Report, 2015; BP, 2023). According to the BP Energy Outlook 2017 edition, dependence on oil and coal is projected to drop to below 30 % of total primary energy by 2035. Meanwhile, the demand for natural gas is expected to rise significantly, potentially overtaking coal and securing its position as the second-largest primary energy source, following oil. Fig. 1 illustrates the projected growth in shares of primary energy sources by the year 2035 (BP, 2017).

Liquefied natural gas technology (LNG) is implemented as a cost-effective alternative for pipelines for overseas transportation of natural gas (Raeisdanaei et al., 2022). This process involves cooling natural gas to approximately −162 °C at atmospheric pressure, making LNG about 1/600th the volume of natural gas at the burner tip. The next subsections provide a thorough overview of the development of LNG processes and optimization studies that were conducted on the C3MR process with a detailed explanation of the research gaps that are addressed in this study.

1.1. Development of LNG processes

Over the decades, LNG liquefaction technology has undergone remarkable transformations, evolving through five distinct stages. With an increased emphasis on heat integration and cogeneration, these advancements underscore the industry's commitment to efficiency and environmental concerns (Bosma and Nagelvoort, 2009);Fig. 2 summarizes the LNG liquefaction development over 5 stages. The LNG liquefaction processes can be categorized based on the used refrigerants and

* Corresponding author.
E-mail address: sahmed@qu.edu.qa (S.F. Ahmed).

https://doi.org/10.1016/j.ces.2024.120560
Received 25 January 2024; Received in revised form 5 July 2024; Accepted 24 July 2024
Available online 26 July 2024

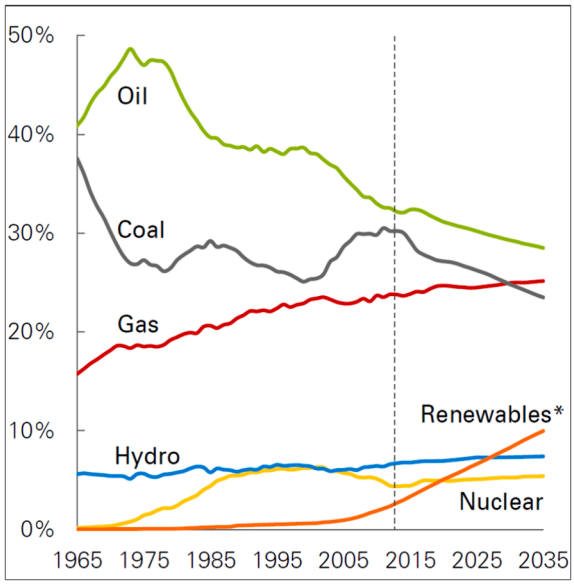

Fig. 1. NG demand increase compared to other primary energy sources (BP, 2017).

cycle configuration into three main groups including cascade, mixed refrigerant (MR), and expander-based (EXP) processes (Mokhatab et al., 2013). Table 1 provides a comprehensive comparison between the future and limitations of these processes. MR processes stand out as more attractive, providing an optimal solution for both onshore and offshore applications on small-large scales (Al-Mutaz et al., 2016). Notably, the C3MR process developed by Air Products, accounting approximately 81 % of the world's baseload LNG production capacity (Khan et al., 2017). In addition, it exhibits a lower specific energy consumption, averaging 10 % less than the cascaded process and 55 % less than the N2 expander-based processes (Furda et al., 2022). However, the energy consumption of these processes is still very high (about 8–10 % of the LNG energy content is consumed during the liquefaction process). Therefore, various studies are actively seeking ways to optimize its energy performance (see Section 1.2) to increase the economic benefits of these processes and concurrently mitigate their negative environmental impacts.

Table 1
LNG liquefaction processes comparison.

Process	Advantages	Limitations	SEC (kWh/kg_{LNG})
Cascade (Lim et al., Mar. 2013)	• High capacity • Efficient operation	• High capital costs • Complex configuration	0.33–0.39 (Furda et al., 2022)
SMR (Khan et al., 2017)	• Simple design • Reduced capital cost • Small footprint	• Lower efficiency • Limited scalability • Flammable refrigerants	0.30–0.40 (Zhang et al., 2020)
C3MR (Khan et al., 2017); (Park et al., 2022)	• Dominance in LNG production (81 %) • High efficiency	• Less attractive for offshore applications • Large propane inventory	0.29–0.30 (Zhang et al., 2020)
DMR (Khan et al., 2017); (Lim et al., 2013)	• Removing limitations on the C3 compressors • Increased capacity	• Complex configuration	0.28–0.30 (Zhang et al., 2020)
Single N_2 Expander (Khan et al., 2017)	• Simplicity • High isentropic efficiency	• High compression energy requirements	0.40–0.97 (Zhang et al., 2020)
Double N_2 Expander (Lim et al., 2013)	• Flexibility with refrigerants	• Increased HXs' size • Safety considerations	0.39–0.56 (Furda et al., 2022)

1.2. Literature review of optimization studies of LNG processes

As summarized in Table 2, numerous researchers have concentrated their optimization efforts on minimizing the specific energy consumption (SEC) value of the C3MR. Other papers have addressed multiple objective functions, with Wang et al. (Wang et al., 2013) as an example. Their objective function incorporates SEC, exergy efficiency (EXE), and Operating expenditures (OPEX). To facilitate the optimization process, the research has employed distinct approaches, broadly categorized as software-based and knowledge-based methods. Numerous studies have utilized a genetic algorithm (GA) approach, as seen in (Alabdulkarem et al., 2011; He and Lin, 2020; Ghorbani et al., 2016), coupled with the Aspen HYSYS software. This combination enables the optimization of the cycle with direct feedback from HYSYS. GA is anticipated to discover the global minimum solution, even in scenarios where the objective function exhibits multiple extrema (Yang et al., 2005). Furthermore, Sabbagh et al. (Sabbagh et al., 2021), Furda et al. (Furda et al., 2022)

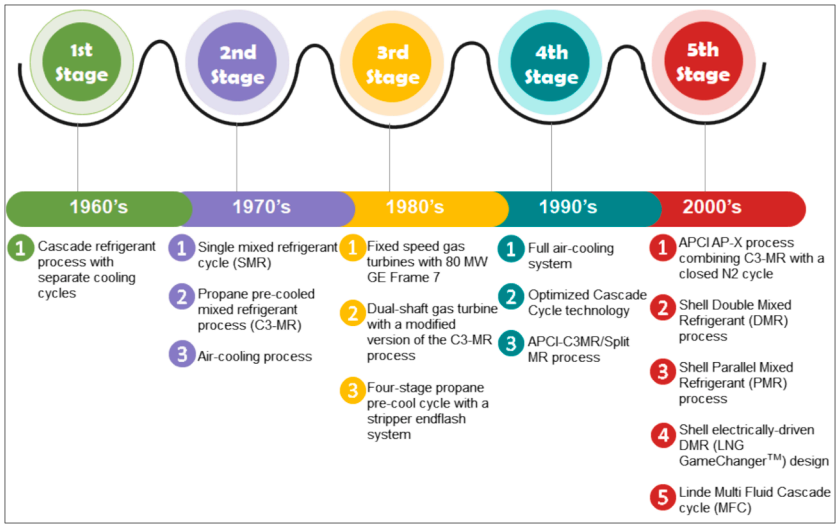

Fig. 2. A historical review of the design development of liquefaction technologies for base load LNG plants.

Table 2
Summary of the optimization studies developed on the C3MR.

Refs.	Year	Process	Approach	Objective function(s)	SEC, kWh/kg	Energy saving, (%)	Software
(Alabdulkarem et al., 2011)	2011	C3MR	GA	SEC	0.283	9.08	MATLAB+HYSYS
(Wang et al., 2011)	2011	C3MR	SQP	SEC	NA	13.70	Aspen Plus
(Husnil et al., 2012)	2012	C3MR	Plantwide	SEC	NA	NA	Aspen Hysys
(Lee, et al., 2012)	2012	C3MR	Case studies	SEC	NA	27.70	NA
(Sun et al., 2012)	2012	C3MR	HYSYS opt.	SEC	NA	9.02	HYSYS
(Wang et al., 2012)	2012	C3MR	MINLP	SEC	NA	13.00	GAMS
(Wang et al., 2013)	2013	C3MR, C3MR-SP	Sequential search	SEC, EXE, OPEX	0.408	NA	Aspen HYSYS
(Khan et al., 2013)	2013	C3MR	KBO	SEC, EXE,	0.278	13.68	Aspen HYSYS
(Wang et al., 2014)	2014	DMR, C3MR	NA	SEC, TCI, TAC, TCC	0.644	26.70, 14.50	Aspen HYSYS
(Khan et al., 2015)	2015	SMR, C3MR	SCRS	SEC	0.475, 0.284	15.00, 14.00	Aspen HYSYS+MS
(Lee et al., 2015)	2015	C3MR	SQP	SEC	0.273	16.40	gPROMS
(Ghorbani et al., 2016)	2016	C3MR	GA	Unit Cost, EXE,	0.259	NA	HYSYS+MATLAB
(Sanavandi and Ziabasharhagh, 2016)	2016	C3MR	HYSYS opt.	SEC	0.271	5.24	Aspen HYSYS
(Sun et al., 2016)	2016	AP-X	GA	SEC	0.271	15.560	MATLAB+HYSYS
(Hajji et al., 2019)	2019	C3MR	DSM	SEC	0.235	11.700	Aspen HYSYS
(Primabudi et al., 2019)	2019	C3MR	GA	EXE, TC	0.837	15.11	Aspen Plus
(Rao et al., 2019)	2019	C3MR	DDNP+GA	SEC	NA	NA	HYSYS
(Song et al., 2019)	2019	C3MR	EDR, SQP	ED	0.252	17.70	MATLAB+HYSYS
(He and Lin, 2020)	2020	C3MR	GA	SEC	NA	16.23	HYSYS
(He and Lin, 2020)	2020	C3MR	GA	SEC	0.440	NA	HYSYS
(Katebah et al., 2020)	2020	C3MR	SQP	SEC	0.277	6.00	Aspen Plus
(Qyyum, 2020)	2020	C3MR, SMR	VSA	SEC	0.260, 0.370	27.80, 16.10	MATLAB+HYSYS
(Veldandi and Kurian, 2020)	2020	C3MR		SEC	0.217	13.85	AVEVA SimCentral
(Sabbagh et al., 2021)	2021	C3MR	GA, NSGA-II	AP, SEC, EXE	0.347	NA	NA
(Cao et al., 2021)	2021	mini-LNG	KBO	Capacity, cost	NA	NA	Aspen HYSYS
(Jin et al., 2022)	2022	N2MR	GA	SEC	0.368	3.20	MATLAB+HYSYS
(Furda et al., 2022)	2022	C3MR	GA, NSGA-II	LPC, CO_2	0.310		MATLAB+HYSYS
(Sun et al., 2022)	2022	SMR, DMR, C3MR, CMR	GA, PSO, BOX	SEC, EXE	0.323, 0.235, 0.249, 0.243	13.30, 15.98, 36.59, 19.53	MATLAB+HYSYS
(Pereira et al., 2022)	2022	SMR, C3MR, DMR, CMR,AP-X	PSO	SEC	0.256, 0.255, 0.246, 0.253,0.237	NA	MATLAB+HYSYS
(Santos et al., 2023)	2023	SMR, C3MR	NSGA-II	SEC, UA	0.217	NA	MATLAB+HYSYS+ GMAS

and Santos et al. (Santos et al., 2023) adopted NSGA-II (Non-dominated sorting genetic algorithm II), which is employed to find optimal solutions for dual and triple objective optimizations. Additionally, another algorithm implemented in various studies is the sequential quadratic programming (SQP) optimization algorithm (Wang et al., 2011; Lee et al., 2015; Katebah et al., 2020). The popularity of SQP methods has grown due to their generality, robustness, and efficiency. In 2022, Sun et al. (Sun et al., 2022) attempted to compare the performance and accuracy of various optimization algorithms, namely GA, PSO, and BOX. Their study revealed that the PSO-optimized LNG process exhibited the best performance. For the knowledge-based optimization (KBO) approach, only one study (Khan et al., 2013) implemented this approach where the researcher's expertise in thermodynamics was leveraged to derive a robust solution based on observed results during the optimization process.

1.3. Technical and methodological gaps in C3MR optimization studies

As identified in the literature review, several technical and methodological gaps exist in the above optimization studies, which can be summarized as follows:

(i) Impractical constraints and assumptions considered in optimization problems. For example, the unbounded minimum internal temperature approach in heat exchangers such as in (Wang et al., 2013) results in an impractical heat exchanger area for real plant implementation. Additionally, some researchers consider wet conditions in compressor inlet streams, introducing potential issues like compressor surge, efficiency loss, component erosion, corrosion, increased motor load, and reduced lubrication effectiveness. Furthermore, certain assumptions in the literature, such as assuming high isentropic efficiency for compressors (e.g., 83 % in (Hajji et al., 2019), may not align with real-world conditions. Therefore, the low SEC values in these studies are due to the high compressor efficiencies and not for the optimization analyses. Moreover, some assumptions made in the literature, like assuming a high isentropic efficiency for compressors (for example, 83 % in reference (Hajji et al., 2019), may not reflect real-world conditions. Consequently, the low SEC values reported in these studies result from the assumed high efficiencies of the compressors rather than from optimization analyses. Therefore, a comparison of the optimized results with these studies must be conducted at the same efficiencies to assess the validity and effectiveness of the optimization methods.

(ii) Most papers considered only one optimization approach or incorporated two approaches to complement each other. However, only a few highlighted the accuracy of their results by comparing different optimization approaches simultaneously. For instance, Sun et al. (Sun et al., 2022) recommended using the PSO algorithm after demonstrating its superiority over GA and BOX approaches.

1.4. Contributions and manuscript organization

To the author's knowledge, integrating the KBO with the CBO to optimize the performance of the cryogenic process is proposed for the

first time in this study. This innovative integration harnesses the robustness of KBO in conjunction with the constraint-handling capabilities of CBO, offering a novel approach to enhancing process efficiency. In particular, for the most common LNG production process (C3MR), this optimization study aims to determine its optimal operation (minimum compression power) under real and rigorous optimization constraints, which are mostly overlooked in previous studies. This study incorporates three distinct novel aspects as follows:

- Performing a systematic knowledge-based optimization (KBO) approach to a large-scale C3MR liquefaction process, which has not been employed in previous studies.
- Proposing the constrained Bayesian optimization (CBO) technique to optimize the performance of large-scale C3MR process.
- Conducting a comparative analysis to assess and contrast the outcomes achieved through the CBO approach with those attained using the KBO method.

Moreover, this study emphasizes the importance of realistic operating conditions to ensure the optimization process yields practical and credible results. These conditions will encompass the establishment of reasonable values for compressor efficiencies, rigorous constraints for the refrigerant quality at the compressors' inlet, and a bounded internal temperature approach of the process heat exchangers. A detailed description of the C3MR process is provided in Section 2. The process simulation and optimization formulation are explained in Section 3. The results of the optimization process using KBO and CBO are discussed and compared in Section 4. Finally, the key findings of this study are summarized in Section 5.

2. C3MR process description

This section describes the C3MR process (shown in Fig. 3) and its operation. The natural gas is fed to the process (stream 43) at 25 °C and 65 bar. Next, the NG is precooled through four heat exchangers (HX-1 to HX-4) as part of the C3 cycle. Afterward, the NG is further cooled in HX-5 and HX-6, then throttled through (V7) to the liquefaction temperature of −162 °C. Finally, the NG passes through a separator (FT-5) to separate the liquefied natural gas (LNG, stream 5) from the remaining flash gas (stream 6).

In the MR cycle, the refrigerant enters HX-1 at stream 7 (at 31.85 °C, and 48.60 bar) and exits from HX-4 at stream 11. The MR then proceeds to a separator (FT-4), where it's split into two streams, streams 12 and 18 that are responsible for the cooling duty of HX-5 and HX-6. Then, the MR is compressed from the low-pressure side to the high-pressure side through an intercooled compression process in compressors C-5 and C-6. In the C3 cycle, Propane (C3) enters the throttling valve (V4) at (40 °C, 14 bar) and expands to lower pressure to perform the cooling duty of HX-1. The exit stream (24) is split into liquid (25) and vapor (40) streams. The liquid stream is further expanded to lower pressure to perform the cooling duty of HX-2 while the vapor stream is directed to be compressed in C-4. The same process is repeated for the exit streams from HX-2 and HX-3. Finally, the exit stream from HX-4 is redirected to C-1 to be compressed to the higher pressure, mixed with vapor streams, and compressed again until reaching the high pressure of the cycle at the outlet of C-4.

3. Modeling and simulation methods

This section presents the definitions of the performance indicators that are used to evaluate the performance of the C3MR process (Section 3.1). Then, the details of optimization formulation (including objective functions, decision variables, constraints, and optimization techniques) are presented in Section 3.2. After that, the details of the process modeling and validation are presented in Section 3.3.

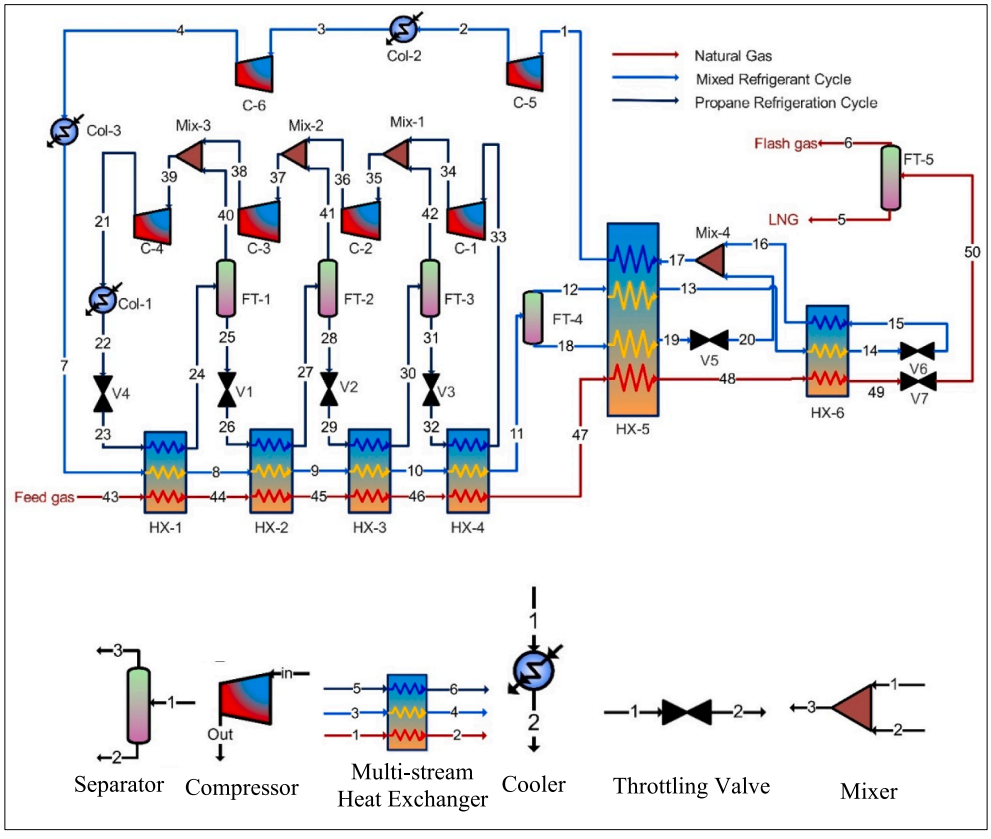

Fig. 3. Layout of the C3MR LNG process.

3.1. Performance indicators

Energetic analysis provides critical information that can be used to optimize the performance of a process, reduce costs, and minimize its environmental impact. Therefore, in this study, the energetic performance of the C3MR liquefaction process will be measured using two performance indicators, which are: the SEC and the coefficient of performance (COP). These performance indicators play a pivotal role in evaluating the efficiency and effectiveness of this cryogenic process. SEC quantifies the energy required to produce a unit of liquefied natural gas, providing insight into the process's energy efficiency. Eq. (1) displays the formula for SEC (Sabbagh et al., 2021).

$$SEC\left(\frac{kWh}{kg}LNG\right) = \frac{\sum W_i(kw)}{\dot{m}_{NG}\left(\frac{kg}{hr}\right)} \tag{1}$$

Where $\sum W_i$ represents the power consumption of individual components or processes within the LNG production system, and $\dot{m}_{NG}$ is the mass flow of the NG which is equal to 120 kg/s in this study. COP measures the effectiveness of energy utilization, representing the ratio of useful cooling or liquefaction achieved to the energy input. Eq. (2) displays the formula for COP (Sleiti and Al-Ammari, 2023).

$$COP = \frac{\sum_{i=1}^{i=6} Q_{HX,i}}{\sum_{j=1}^{j=6} \dot{W}_{C-j}} \tag{2}$$

where $\sum_{i=1}^{i=6} Q_{HX,i}$ represents the total cooling load of the C3MR heat multi-stream heat exchangers and can be expressed as follows (Sleiti and Al-Ammaria, 2024):

$$\sum_{i=1}^{i=6} Q_{HX,i} = Q_{HX,1} + Q_{HX,2} + Q_{HX,3} + Q_{HX,4} + Q_{HX,5} + Q_{HX,6} \tag{3}$$

and $\sum_{j=1}^{j=6} \dot{W}_{C-j}$ represents the total compression power of the C3MR compressors and can be expressed as follows:

$$\sum_{j=1}^{j=6} \dot{W}_{HX,j} = \dot{W}_{C-1} + \dot{W}_{C-2} + \dot{W}_{C-3} + \dot{W}_{C-4} + \dot{W}_{C-5} + \dot{W}_{C-6} \tag{4}$$

3.2. Optimization formulation

The details of the optimization formulation of this study are presented in this section.

3.2.1. Objective functions

The primary goal of this research is to enhance the efficiency of the C3MR liquefaction process by reducing SEC. A lower SEC value signifies improved energy efficiency, making it the focus of the objective function, defined as follows (Sleiti et al., 2023):

$$Objectivefunction: Minimize(SEC) = \frac{\sum W_i}{\dot{m}_{NG}} \tag{5}$$

3.2.2. Decision variables

To optimize the predefined objective functions, some decision variables will be selected, which are the parameters or variables subject to adjustment or control to attain particular objectives and enhance specific outcomes. These selected decision variables involve the low and high-pressure streams in both the C3 cycle and MR cycle, along with the mass flow rates of C3 and MR (as shown in Table 3), as well as the mass fraction of MR components. The initial and optimized values (which are determined based on the optimal results of this study) of each variable are reported in Table 3 to facilitate the comparison process between them. The optimal composition of the mixed refrigerant is provided later in Table 9.

Table 3
Decision pressure and mass flow variables of the C3MR process.

Variable	Range	Initial value	Optimized value
C3 cycle			
P_{23}, (bar)	6.5–8.5	7.2	7.7
P_{26}, (bar)	4.0–7.0	5.1	5.6
P_{29}, (bar)	1.5–3.5	2.5	2.75
P_{32}, (bar)	1.0–2.0	1.3	1.31
P_{21}, (bar)	12.0–16.0	14.3	13.98
C3 mass flow, (kg/h)	350–550	446	441.5
MR cycle			
P_{15}, (bar)	1.0–4.0	3.0	3.45
P_2, (bar)	15.0–25.0	21.0	21.0
P_4, (bar)	35.0–55.0	48.6	48.6
MR mass flow, (kg/h)	180—360	300	294

3.2.3. Optimization assumptions & constraints

The details of the optimization constraints are presented in Table 4. Concerning constraints, two were taken into account for the six centrifugal compressors in the C3MR. One constraint requires the MR entering the compressor to be in a vapor phase, while the other dictates that the pressure ratio of the compressor must fall within the range of 1.3 to 7. In the case of the six multi-stream heat exchangers within the cycle, it is essential to maintain a minimum internal temperature approach (MITA) ranging from 0.5 to 4. This ensures both high efficiency and performance of the heat exchangers while striving to minimize costs, striking a balance between efficiency and cost. Furthermore, to ensure the feasibility of mixing streams in the mixers of the C3 cycle (Mix-1 to Mix-3, Fig. 3) and MR cycle (Mix-4, Fig. 3), the pressure of the inlet streams for each mixer must be equal as shown in the last row of Table 4.

As for the assumptions, this study operates under steady-state conditions. Additionally, it is assumed that the compressors' adiabatic efficiency is 75 %, which are realistic values attainable in real-world compressor operations. Furthermore, phase separators, heat exchangers, air coolers, and mixers are assumed to operate without any pressure drops. The fed NG is made up of different gases, including nitrogen (N_2), methane (CH_4), ethane (C_2H_6), propylene (C_3H_6), and n-butane with the following mass fractions (N_2: 0.0615, CH_4:0.7684, C_2H_6: 0.0906, C_3H_6: 0.0512, n-Butane: 0.0283).

3.2.4. Optimization techniques

Two innovative optimization techniques are adopted in this study. These techniques encompass knowledge-based optimization (KBO) and constrained Bayesian optimization (CBO), a comprehensive explanation of both approaches is given in the following subsections.

The optimization of SEC for the C3MR liquefaction cycle is carried out systematically using the KBO approach. The optimization process is performed sequentially, beginning with the C3 cycle, followed by the MR cycle, and concluding with the MR composition. Within the C3 cycle, the following steps were followed as summarized in Fig. 4.

1) First, we Increase the low-pressure (LP) of the evaporator streams in the C3 cycle, aiming to reduce the pressure difference between the inlet and outlet of the compressors, which may decrease the load on the compressors.

Table 4
Optimization constraints & assumptions.

Constraints	Justification
$f_{vap,i}^{C_k} = 1$	To prevent compressors' operational issues.
$0.5 \leq MITA \leq 4$	To ensure valid, feasible, and efficient HX design.
$1.3 \geq Pr \leq 7$	To be within the practical range of commercial compressors.
$P_{34} = P_{42}$, $P_{36} = P_{41}$, $P_{38} = P_{40}$, $P_{15} = P_{20}$	To ensure that the mixed streams (in Mix-1 to Mix-4) are mixed at the same pressure

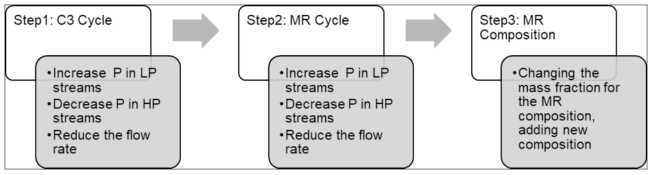

Fig. 4. KBO methodology.

2) At each set for the LP, we decrease the high-pressure (HP) in the C3 cycle to reduce the work needed by the compressors.
3) At each optimal set for the LP and HP values, we reduce the C3 flow rate, to reduce the load on the compressors, which are contributing the most to the power consumption by the whole loop.

These adjustments aim to minimize the SEC value while maintaining the C3 cycle's integrity, avoiding issues like temperature cross in the heat exchangers or liquid in inlet streams of the compressors, etc. Similarly, in the MR cycle, the same approach is applied starting with the increase in the LP and then the decrease in the HP, followed by the reduction in the MR flow. The minimum SEC value obtained after optimizing the C3 and MR cycle pressure streams will serve as the reference case for the fourth step: optimizing the mixed refrigerant composition (using CBO). The optimization of the MR composition is performed by tuning the heavyweight and lightweight refrigerant fractions in the basic mixture. Additionally, new components, not present in the basic mixture, are also introduced to the MR composition.

The MR comprises two categories, as detailed in (Sleiti and Al-Ammari, 2022): lightweight components (including N2, CH4, C2H6, and R14) and heavyweight components (C3H8, n-C4H10, i-C4H10, i-C5H12, and n-C5H12). Lightweight components have boiling points below −100 °C and freezing points under −168 °C, making them responsible for achieving very low cryogenic temperatures in the liquefaction process (e.x. in HX6). In contrast, heavyweight components have boiling points higher than −88 °C and freezing points (except C3H8) higher than −160 °C, which make them responsible for providing the primary refrigeration effect (cooling capacity) through the pre-cooling process (e.x. in HX5). The heavyweight/ lightweight components of the MR that are considered in this study are summarized in Table 5 as reported in (Sleiti and Al-Ammari, 2022). The data of the boiling and triple point temperatures are obtained from the library of engineering equation solver (EES) library. The boiling point of each component is obtained as the saturation temperature at a pressure of 1.0 bar.

The systematic optimization of mass fractions for MR components has been carried out following the following procedures (Sleiti and Al-Ammari, 2022):

Table 5
Thermophysical properties of the pure components of candidate refrigerants (Sleiti and Al-Ammari, 2022).

Component	Boiling point temp. [°C]	Triple point temp. [°C]
Lightweight components		
Nitrogen (N2)	−195.80	−210.00
Methane (CH4)	−161.50	−182.50
Ethane (C2H6)	−88.59	−182.80
Refrig-14 (R14)	−127.90	−183.60
Heavyweight components		
Propane (C3H8)	−42.10	−187.70
n-Butane (n-C4H10)	−0.53	−138.30
i-Butane (i-C4H10)	−11.68	−159.60
i-Pentane (i-C5H12)	27.85	−160.50
n-Pentane (n-C5H12)	35.87	−129.70

1) Determine the number of pure components that need to be mixed to develop the MR composition. For LNG production, using four or five refrigerants is usually enough to get the best composition with a target temperature of −162 °C.
2) Decide on the initial flow rate for the total MR stream.
3) Select the initial fractions for the heavy and light refrigerants, considering their properties listed in Table 5 (it is recommended to start with 40 % for light components and 60 % for heavy components).
4) Start initializing the fraction of each component with the intention to increase the heavyweight components since they are easier to be compressed in the cycle, and to decrease the lightweight components in the mixture since they will require more work.
5) Simulate the C3MR process with the new compositions to check if the developed MR is valid or not. Valid MR means that there is no thermophysical problem (no temperature-cross and/or no overlaps on the composite curves, and no liquid in compressors' inlet streams).
6) Tune the MR flow to get the minimum possible value for SEC while maintaining the cycle without any problems.

Bayesian optimization is a sophisticated technique designed for optimizing functions with costly evaluations, especially in scenarios where the objective function lacks a known mathematical expression. At its core, Bayesian optimization employs a probabilistic model, often a Gaussian process (GP), to approximate the unknown function. The Gaussian process model is used because it provides a flexible and robust way to model complex functions. The GP is defined by a mean function $\mu(x)$ and a covariance function $k(x,x')$. Given a set of observations, the GP can predict the function value at a new point by calculating the mean and variance of the predicted function values, incorporating both the prior mean and the observed data as follows (Rasmussen et al., 2006):

$$\mu(x) = K(x,X)\left(K(X,X) + \sigma^2 I\right)^{-1} y \tag{6}$$

$$\sigma^2(x) = k(x,x') - K(x,X)\left(K(X,X) + \sigma^2 I\right)^{-1} K(X,x) \tag{7}$$

where X is the set of input points, y is the set of observed function values, K is the covariance matrix of the training points, and σ^2 represents the noise in the observations. This model captures the belief about the function's behavior based on available data by updating the mean and variance at each step with new observations. The function $k(x,x')$ is known as the covariance or kernel function, and it describes the spatial or temporal covariance of a random variable process. There are various types of kernel functions, such as the squared exponential, exponential, linear, and spherical kernels. Although the squared exponential kernel is commonly used, it is often too smooth for practical optimization problems. Previous studies have shown that the Matérn 5/2 kernel provides a more optimized solution. Therefore, this study adopts the Matérn 5/2 kernel, which is expressed as follows (Noh et al., 2022):

$$k(x,x') = \left(1 + \frac{\sqrt{5}\ d(x,x')}{l} + \frac{5d(x,x')^2}{3l}\right)\exp\left(-\frac{\sqrt{5}\ d(x,x')}{l}\right) \tag{8}$$

where $d(x,x')$ denotes the Euclidean distance and l denotes the length scale hyper-parameter. The balance between exploration (searching in regions with high uncertainty) and exploitation (searching in regions likely to contain the optimum) is achieved through the use of an acquisition function. The acquisition function guides the selection of the next point to evaluate by considering both the predicted mean and uncertainty (variance) from the GP model. Common acquisition functions include Expected Improvement (EI), Probability of Improvement (PI), and Upper Confidence Bound (UCB). For instance, the Expected Improvement (EI) function is defined as (Noh et al., 2022):

$$\mathrm{EI}(x) = E[\max(f(x) - f(x^+), 0)] \tag{9}$$

where $f(x^+)$ is the best function value observed so far. The point that maximizes the EI function is selected for the next evaluation. Another form of the EI function is given by:

$$EI(x) = \sigma(x)(\gamma(x)\Phi(\gamma(x)) + \phi(\gamma(x))) \tag{10}$$

where $\sigma(x))$ denotes the standard deviation of the posterior predictive at x , and Φ and ϕ denote the cumulative distribution function (CDF) and the probability density function (PDF) of the standard normal distribution, respectively. The CDF is related to exploitation, while the PDF is related to exploration. The term $\gamma(x)$ is defined as:

$$\gamma(x) = \frac{\mu(x) - f(x^+) - \xi}{\sigma(x)} \tag{11}$$

where ξ is a parameter that determines the trade-off between exploration and exploitation. A larger ξ value favors exploration, while a smaller ξ value favors exploitation. In this study, ξ was set to 0.02. The Bayesian optimization process unfolds iteratively, following these steps:

(i) *Initialization*: The process begins with an initial set of evaluations, which are used to fit the initial Gaussian process model.
(ii) *Acquisition function optimization*: The algorithm optimizes the acquisition function to determine the next point for evaluation. This step involves balancing exploration and exploitation as explained above.
(iii) *Evaluation and update:* The selected point is evaluated on the true objective function, and the model is updated with this new information.
(iv) *Iteration:* Steps (ii) and (iii) are repeated until a stopping criterion (such as a maximum number of iterations) is met.

Through this iterative process, Bayesian optimization efficiently explores the search space, gradually refining its understanding of the objective function and converging to the optimal solution while minimizing the number of costly evaluations.

In the CBO, the optimization process begins by optimizing the MR compositions (Step 4 in the KBO) and mass flow to reach the lowest possible SEC value. The CBO approach builds on the insights gained from the researcher's experience with the KBO approach, aiming to automate and enhance the process. Fig. 5 illustrates the flowchart of the CBO algorithm, beginning with the initialization of the optimization process. The algorithm establishes a connection with ASPEN HYSYS V12 and proceeds to read the user decision variables targeted for optimization, along with the constraints defining their allowable ranges. The Bayesian optimization technique acts as the optimization agent in this scenario.

The program then enters a loop to monitor the user-specified iteration limit. If the limit is not reached, the algorithm proceeds to the query acquisition function. Upon acquiring a new set of parameters, involving a modified composition of the MR, the HYSYS parameters are adjusted. Changes in the objective function and other parameters are calculated based on the new composition and mass flow. The algorithm assesses user-defined constraints, prints the updated SEC value, and iterates the process until reaching the specified iteration limit. Upon reaching the limit, the loop terminates, and the algorithm saves the generated results, indicating the end of the optimization process. Fig. 6 provides a short version of the CBO algorithm, offering a simplified and easily understandable representation of the logic described in the flowchart.

3.3. Process simulation and validation

In this study, Aspen HYSYS software is employed to model and simulate the C3MR) cycle. The Peng-Robinson equation of state is judiciously selected for its suitability for the thermodynamic properties of the refrigerants at cryogenic temperatures (Bozorgkhou et al., 2022);

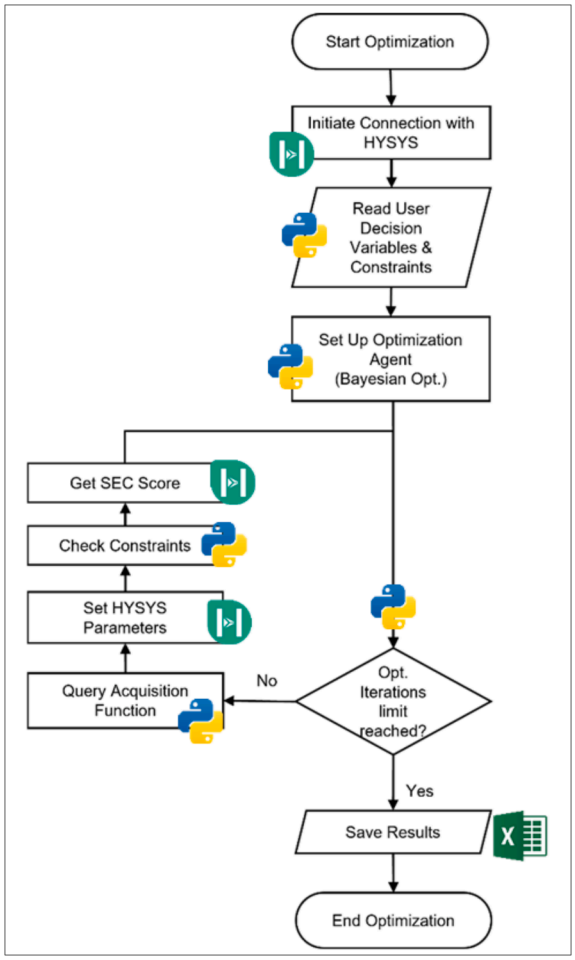

Fig. 5. CBO flowchart.

Algorithm 1: Constrained Bayesian Optimization Algorithm.

```
Data: hysys_prog, const, limits, num_iter
Result: optimiztion_results
conn ← Conn(hysys_prog);
conn.init_conn();
const ← setup_const_func(const);
opt_agent ← BOA(const, limits);
opt_agent.setup_acq_func();
while i in range num_iter do
    next_params ← opt_agent.query_next_params();
    conn.set_params(next_params);
    const_status ← conn.check_const();
    sec ← conn.get_sec();
    opt_agent.update_model(const_status, sec);
end
results ← opt_agent.get_results();
save_to_disk(results);
```

Fig. 6. Short version of CBO algorithm.

(Shayan et al., 2020). The key parameters of the C3MR process are detailed in Table 6.

Before introducing the optimization procedure for the C3MR process, the simulation of the C3MR process is validated. This validation involved a meticulous comparison of the model's performance against the findings of Ghorbani et al. in (Ghorbani et al., 2016), specifically focusing on identical compositions for natural gas (NG) and mixed refrigerant (MR) as outlined in Table 7. Additionally, the process also

Table 6
Key operating parameters of the C3MR process (base case).

Stream	Temp.	Pressure	Mass flow	Composition (Mole fractions)				
	K	bar	kg/h	N_2	CH_4	C_2H_6	C_3H_8	C_4H_{10}
1	230.6	3.0	97.38	0.0700	0.4181	0.2989	0.2130	0.0000
2	364.5	21.0	97.38	0.0700	0.4181	0.2989	0.2130	0.0000
3	303.2	21.0	97.38	0.0700	0.4181	0.2989	0.2130	0.0000
4	368.6	48.6	97.38	0.0700	0.4181	0.2989	0.2130	0.0000
5	107.1	1.0	45.34	0.0154	0.8932	0.0591	0.0228	0.0096
6	107.1	1.0	3.836	0.3712	0.6287	0.0000	0.0000	0.0000
7	305.0	48.6	97.38	0.0700	0.4181	0.2989	0.2130	0.0000
8	290.6	48.6	97.38	0.0700	0.4181	0.2989	0.2130	0.0000
9	278.8	48.6	97.38	0.0700	0.4181	0.2989	0.2130	0.0000
10	256.8	48.6	97.38	0.0700	0.4181	0.2989	0.2130	0.0000
11	240.0	48.6	97.38	0.0700	0.4181	0.2989	0.2130	0.0000
12	240.0	48.6	21.82	0.1704	0.6554	0.1410	0.0331	0.0000
13	144.7	48.4	21.82	0.1704	0.6554	0.1410	0.0331	0.0000
14	113.0	48.4	21.82	0.1704	0.6554	0.1410	0.0331	0.0000
15	106.5	3.0	21.82	0.1704	0.6554	0.1410	0.0331	0.0000
16	140.7	3.0	21.82	0.1704	0.6554	0.1410	0.0331	0.0000
17	140.2	3.0	97.38	0.0700	0.4181	0.2989	0.2130	0.0000
18	240.0	48.6	75.56	0.0292	0.3217	0.3630	0.2861	0.0000
19	144.8	48.4	75.56	0.0292	0.3217	0.3630	0.2861	0.0000
20	139.1	3.0	75.56	0.0292	0.3217	0.3630	0.2861	0.0000
21	330.3	14.3	163.035	0.0000	0.0000	0.0000	1.0000	0.0000
22	313.1	14.3	163.035	0.0000	0.0000	0.0000	1.0000	0.0000
23	287.6	7.2	163.035	0.0000	0.0000	0.0000	1.0000	0.0000
24	287.6	7.2	163.035	0.0000	0.0000	0.0000	1.0000	0.0000
25	287.6	7.2	107.853	0.0000	0.0000	0.0000	1.0000	0.0000
26	275.6	5.1	107.853	0.0000	0.0000	0.0000	1.0000	0.0000
27	275.6	5.1	107.853	0.0000	0.0000	0.0000	1.0000	0.0000
28	275.6	5.1	74.435	0.0000	0.0000	0.0000	1.0000	0.0000
29	253.8	2.5	74.435	0.0000	0.0000	0.0000	1.0000	0.0000
30	253.8	2.5	74.435	0.0000	0.0000	0.0000	1.0000	0.0000
31	253.8	2.5	27.766	0.0000	0.0000	0.0000	1.0000	0.0000
32	236.8	1.3	27.766	0.0000	0.0000	0.0000	1.0000	0.0000
33	242.0	1.3	27.766	0.0000	0.0000	0.0000	1.0000	0.0000
34	268.6	2.5	27.766	0.0000	0.0000	0.0000	1.0000	0.0000
35	259.4	2.5	74.435	0.0000	0.0000	0.0000	1.0000	0.0000
36	290.1	5.1	74.435	0.0000	0.0000	0.0000	1.0000	0.0000
37	285.6	5.1	107.853	0.0000	0.0000	0.0000	1.0000	0.0000
38	301.4	7.2	107.853	0.0000	0.0000	0.0000	1.0000	0.0000
39	296.8	7.2	163.035	0.0000	0.0000	0.0000	1.0000	0.0000
40	287.6	7.2	55.182	0.0000	0.0000	0.0000	1.0000	0.0000
41	275.6	5.1	33.417	0.0000	0.0000	0.0000	1.0000	0.0000
42	275.6	2.5	46.669	0.0000	0.0000	0.0000	1.0000	0.0000
43	300.0	65.0	49.179	0.0401	0.8748	0.0550	0.0212	0.0089
44	290.6	65.0	49.179	0.0401	0.8748	0.0550	0.0212	0.0089
45	278.8	65.0	49.179	0.0401	0.8748	0.0550	0.0212	0.0089
46	256.8	65.0	49.179	0.0401	0.8748	0.0550	0.0212	0.0089
47	237.5	65.0	49.179	0.0401	0.8748	0.0550	0.0212	0.0089
48	144.7	65.0	49.179	0.0401	0.8748	0.0550	0.0212	0.0089
49	113.0	65.0	49.179	0.0401	0.8748	0.0550	0.0212	0.0089
50	107.1	1.0	49.179	0.0401	0.8748	0.0550	0.0212	0.0089

Table 7
Considered compositions for the C3MR feed (NG) and mixed refrigerant (MR).

Component	Composition	
	NG	MR
Nitrogen	0.0401	0.0700
Methane	0.8748	0.4181
Ethane	0.0550	0.2989
Propane	0.0212	0.2130
Butane	0.0089	0.0000

entailed maintaining the same plant capacity, pressure, and temperature values for material streams, as well as ensuring the complete congruence of compressors and heat exchangers.

The selection of Ghorbani et al.'s study for comparison was motivated by their comprehensive disclosure of all parameters relevant to the C3MR process, which is essential for the replication of their methodology. The outcomes of this validation, inclusive of key parameters such as feed natural gas flow, LNG flow, SEC, compressor power, and heat exchanger cooling duty, have been concisely compiled in Table 8. Notably, the discrepancies between these parameters and the reference data were exceedingly minimal, with the highest recorded error percentage of 0.9 %. The relative error in the specific power (0.8782 %) is higher than that of the other parameters. This may be explained by that the SEC definitions combined the power of C-1 to C-6, which aggregate and magnify errors of the individual power calculations.

4. Results and discussion

This section aims to present the results obtained throughout the study for optimizing the C3MR liquefaction process. It will begin by discussing the results of the KBO approach. Subsequently, the main findings of the CBO approach will be presented through different case scenarios. A comparative analysis between KBO and CBO, based on the results obtained, will follow, accompanied by some recommendations. Lastly, a comparison between the optimal case and the base case from

Table 8
Verification of the C3MR Model VS. Ghorbani et al. (Ghorbani et al., 2016) results.

Parameter	Ghorbani et al. (Wang et al., 2013)	Present work	Relative. error (%) *
Feed natural gas flow, (kg/h)	49.179	49.179	–
LNG flow, (kg/h)	45.344	45.343	0.00221
Flash gas flow, (kg/h)	3.835	3.836	0.02608
Specific power, (kWh/kg LNG)	0.2594	0.2571	0.87820
Power of C-1, (kW)	0.2861	0.2865	0.13981
Power of C-2, (kW)	0.8797	0.8801	0.04547
Power of C-3, (kW)	0.6462	0.6464	0.03095
Power of C-4, (kW)	1.9399	1.941	0.05670
Power of C-5, (kW)	6.0706	6.07	0.00988
Power of C-6, (kW)	2.8203	2.821	0.02482
Cooling duty of HX-1, (kJ/h)	7763	7759	0.05153
Cooling duty of HX-2, (kJ/h)	9092	9093	0.01100
Cooling duty of HX-3, (kJ/h)	14,730	14,730	0.00000
Cooling duty of HX-4, (kJ/h)	10,755	10,760	0.04649
Cooling duty of HX-5, (kJ/h)	52,041	52,030	0.02114
Cooling duty of HX-6, (kJ/h)	6753	6746	0.10366

* Rel. Error = 100*|Ref. (Ghorbani et al., 2016)– Present work|/Ref. (Ghorbani et al., 2016).

various aspects will be conducted, along with a comparison with the literature. In addition, this section provides a comparison with the industry that utilizes the C3MR process to produce LNG.

4.1. Optimized C3MR performance using knowledge-based optimization

This section will elaborate on the outcomes derived from the KBO following the above three optimization steps (Section 4.1.1) and MR composition (Section 4.1.2).

4.1.1. Optimizing C3/MR operational pressures and flow rates

The optimization process started with a SEC value of 0.3102 kWh/kg_{LNG} and after increasing the LP, decreasing the HP, and adjusting the C3 flow accordingly to avoid any errors in the cycle, the value of the SEC was reduced by around by around 2.15 % at a C3 flow rate of 441.5 kg/s. Fig. 7, illustrates the optimized C3 cycle, providing details on pressure, temperature, and mass flow for each material stream in the optimized scenario.

Regarding the MR Cycle, the optimization procedures align with those employed in the C3 cycle, involving the optimization of process LP, HP, and MR flow rate. However, it has been noted that the influence of the HP in the MR cycle on the SEC is negligible. In contrast, the LP has played a significant role, resulting in a decrease in SEC to 0.2876 kWh/kg LNG, marking a roughly 7.29 % reduction from the base case (0.3102 kWh/kg_{LNG}). This observation implies that the MR cycle has a more pronounced impact on SEC compared to the C3 cycle. Therefore, for the researchers who are looking to further investigate and optimize the C3MR cycle, concentrating on the MR cycle appears promising due to its noticeable effect on cycle efficiency. Fig. 8 depicts the optimized MR cycle, presenting details on pressure, temperature, and mass flow for each material stream in the optimized scenario.

4.1.2. Optimizing the MR composition

The optimization of the MR composition is performed at a constant value for the C3 flow rate, specifically 441.5 kg/s. The highest pressure recorded in the cycle was 48.60 bar, while the lowest was 1.31 bar.

The optimization process started with MR5,1, representing group number 1 consisting of 5 candidate MR components (see Table 9). Four of these components served as the base case: ethane, methane, nitrogen, and propane. An additional component, i-Butane, was introduced. The inclusion of i-Butane initially contributed to a reduction in SEC and MR flow. However, this composition led to the formation of liquid in the inlet streams of the C3 compressors. Moreover, it reduced the temperature at the inlet of Col-3, effectively causing the cooler to function as a heater due to the low temperature of the inlet flow compared to ambient temperature.

Despite multiple attempts to address these issues, solutions increased the SEC value and MR flow. Therefore, the compositions within this group could be advantageous if leveraging the low temperature of the MR in the compressor's inlet has been utilized. This could be achieved by circulating the MR as a cooling agent through a cooler to benefit from the coldness of the MR stream. Consequently, the after-cooler

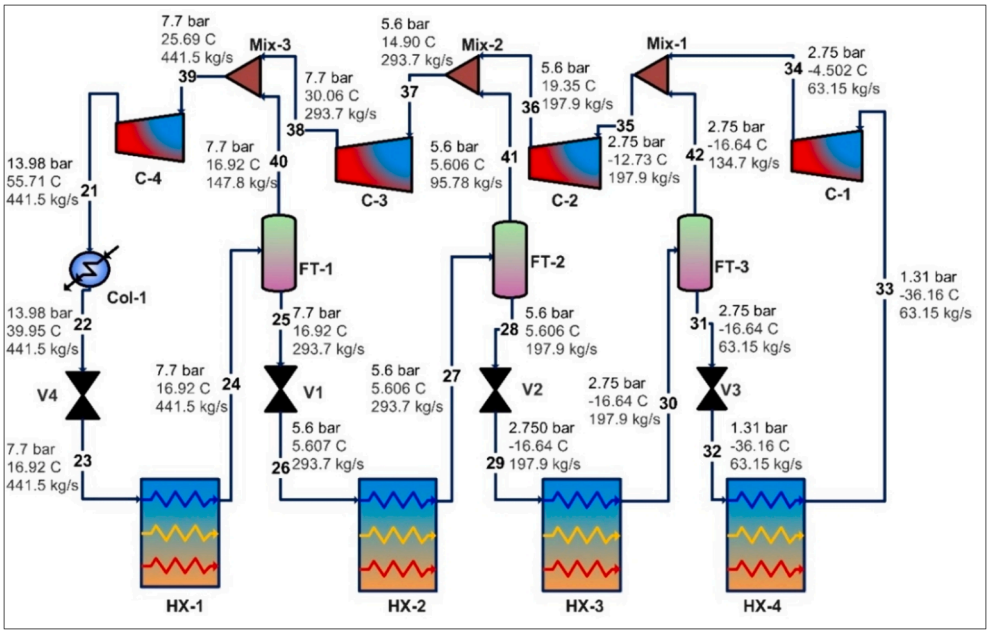

Fig. 7. C3 cycle with optimized values for pressure and mass flow parameters.

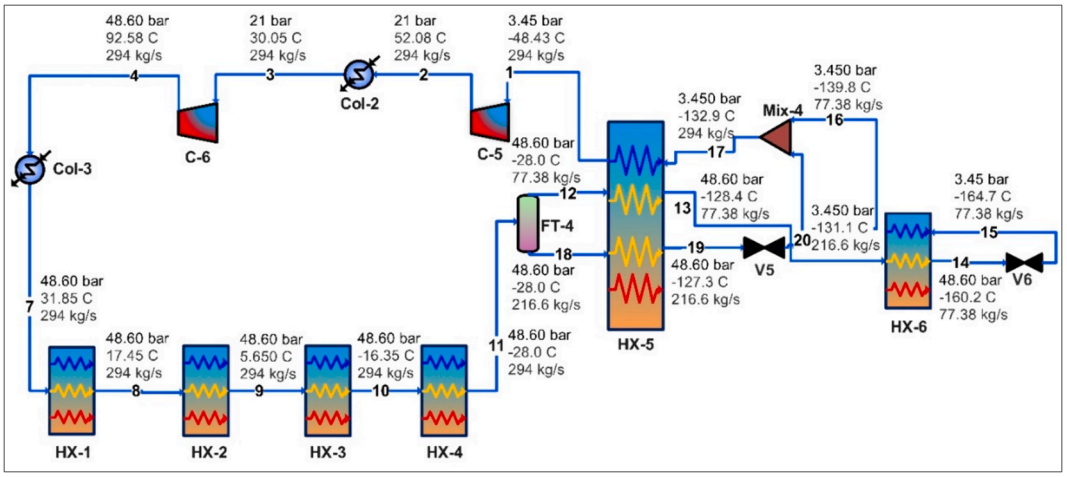

Fig. 8. MR cycle with optimized values for pressure streams and mass flow.

Table 9
Molar fraction-based composition of 12 mixed refrigerant cases using KBO.

Group	Case#*	Candidate MR components							MR flow[kg/s]	SEC[kWh/kg LNG]
		C2H6	R14	CH4	N2	C3H8	i-C4H10	n-C4H10		
Base Case		0.33	0.00	0.25	0.07	0.35	0.00	0.00	446	0.3102
MR5,1**	1	0.25	0.00	0.22	0.06	0.39	0.08	0.00	317	0.2731
	2	0.25	0.00	0.22	0.06	0.41	0.06	0.00	313	0.2715
	3	0.25	0.00	0.22	0.06	0.42	0.05	0.00	310	0.2701
MR5,2	4	0.25	0.00	0.22	0.06	0.20	0.00	0.27	294	0.2484
	5	0.25	0.00	0.22	0.06	0.38	0.00	0.10	320	0.2731
	6	0.25	0.00	0.22	0.06	0.42	0.00	0.05	317	0.2702
MR5,3	7	0.24	0.02	0.22	0.05	0.48	0.00	0.00	301	0.2670
	8	0.24	0.01	0.22	0.06	0.48	0.00	0.00	302	0.2667
	9	0.25	0.03	0.22	0.06	0.48	0.00	0.00	296	0.2658
MR4, 4	10	0.34	0.00	0.24	0.07	0.34	0.00	0.00	294	0.2847
	11	0.35	0.00	0.20	0.07	0.38	0.00	0.00	294	0.2672
	12	0.25	0.00	0.22	0.06	0.47	0.00	0.00	294	**0.2649**

* In all cases, C3 flow is fixed at 441.5 kg/s, HP=48.60 bar, LP=1.31 bar.
** MRn,m, refers to group# m that has #of components equal n.

temperature of the MR would increase before the compression process, eliminating the presence of liquid in the compressor's inlet stream.

In the case of group MR5,2, the mixed refrigerant comprised 5 components similar to group (1). However, i-Butane was substituted with n-Butane, which has a higher weight compared to i-Butane. The SEC value and MR flow were lower than the base case. Nonetheless, HYSYS software reported certain issues, particularly an increase in the cooling temperature of Col-3, similar to group (1). For instance, in case 4, the SEC is reduced to 0.2484 kWh/kg_{LNG}, which is about 12 % lower than the average of the other cases (0.270 kWh/kg_{LNG}). However, in case 4, a temperature cross in MR heat exchangers was observed. This means that the temperature of the cold fluid exceeds that of the hot fluid at certain points in the exchanger, which is not acceptable as it is not a thermodynamically feasible process. This temperature cross makes these compositions not practical as it violates thermodynamic principles.

Moving on to the 3rd group, MR5,3, it also comprised 5 components. In this case, n-Butane from the previous group was substituted with Refrig-14, a component lighter than the two components used in groups (1) and (2). However, these compositions introduced issues in the cycle, including the presence of liquid in the inlet streams for certain compressors. Attempts to troubleshoot these errors required the reduction of the low-pressure streams in the MR loop and an increase in MR flow. This corrective action led to an elevation in the SEC value.

In the 4th group, the number of components was reduced to 4 from the original 5 to simplify the manufacturing complexity of the MR. The components included in group (4) are the same as those in the base case: ethane, methane, nitrogen, and propane. Some trial compositions within this group showed a temperature cross in the MR heat exchangers. However, fine-tuning the MR flow rate proved effective in resolving the issue with the heat exchangers, resulting in an SEC value lower than that of the base case, literature values for similar capacities, and the industrial benchmark.

The case producing the minimum SEC value without violating any constraints is case 12, characterized by the following compositions: [nitrogen: 0.0625, methane: 0.2230, ethane: 0.2230, and propane: 0.4672], with a mass flow of 298 kg/s. Fig. 9 illustrates the SEC values

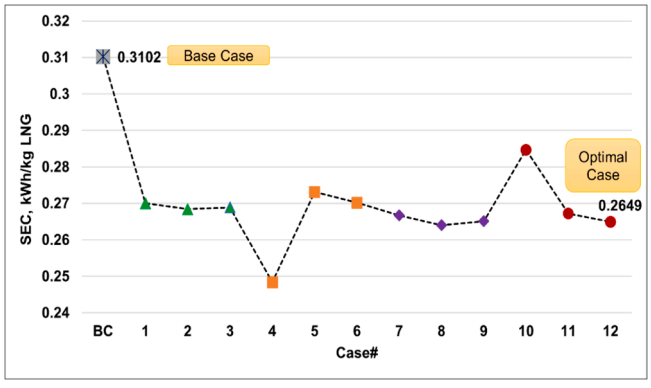

Fig. 9. SEC values for the 12 MR composition cases generated by KBO.

for the 12 cases outlined in Table 9, emphasizing the improvement observed between the base case and the optimal case. In summary, the trials conducted in this section explored various compositions and numbers of components. However, the important results are briefly presented in Table 9. In the optimal case (case #12), the SEC value (0.2649 kWh/kg_{LNG}) is, which is 14.6 % lower than the base case value.

Fig. 10 illustrates the overall MR composite curve for the C3MR process, comparing the base case with the optimal case. The x-axis represents heat flow in MW, and the y-axis represents temperature in °C. The light-yellow shaded portion indicates the performance of the MR heat exchangers, while the light-green shaded portion represents the performance of the C3 heat exchangers. Upon comparing both graphs, it becomes evident that the performance of the MR heat exchangers in the optimal case has improved. This is expressed by the reduction of the gap between the hot and cold composites to almost below 1 °C. A detailed discussion in Section 4.4 will validate that this improvement results from an increase in the overall heat transfer coefficient rather than an increase in the heat exchangers' area. However, a segment of the curve, particularly in the range of 2000–3000 MW heat flow, indicates a potential for further enhancement of these MR heat exchangers to achieve a lower SEC value. Concerning the pure refrigerant, a slight improvement is noticeable in the optimal case compared to the base case.

It's worth noting that MR compressor number 5 (C-5) in Fig. 3, is in wet condition (followed by the model proposed by Ghorbani et al (Wang et al., 2013) with a liquid phase fraction of 0.1. It is also noticed that the MR temperature is still very low at the inlet of C-5. Thus, the coldness of the MR stream could be further utilized in the cycle before compression in C-5. A proposed approach is to get the benefit from the cold energy of the inlet stream of C-5 (stream 1) in the precooling process of the MR using a new shell-tube cooler (Col-4) added to the cycle before Col-2. This modification aims to increase the temperature of stream 1 till it reaches the saturated vapor status before entering C-5, which will help in maintaining a longer lifetime for the compressor, as well, as to have a lower maintenance activity. Also, from another perspective, recovering the cold energy in stream 1 by Col-4 will help to reduce the load on Col-2. As a result, this will minimize the water consumption consumed by Col-2, if the cooler is using the water as a cooling median, or it will reduce the power consumption if the cooler is using the air to cool down the MR. This practical approach has been previously mentioned by Sleiti et al. in (Sleiti and Al-Ammari, 2023). Fig. 11 illustrates a schematic of the proposed cycle modification to benefit from the excessive cooling energy in C-5′s inlet stream 1, with Col-4 representing the new cooler added to the cycle to reduce the load on Col-2, and stream 3‘.

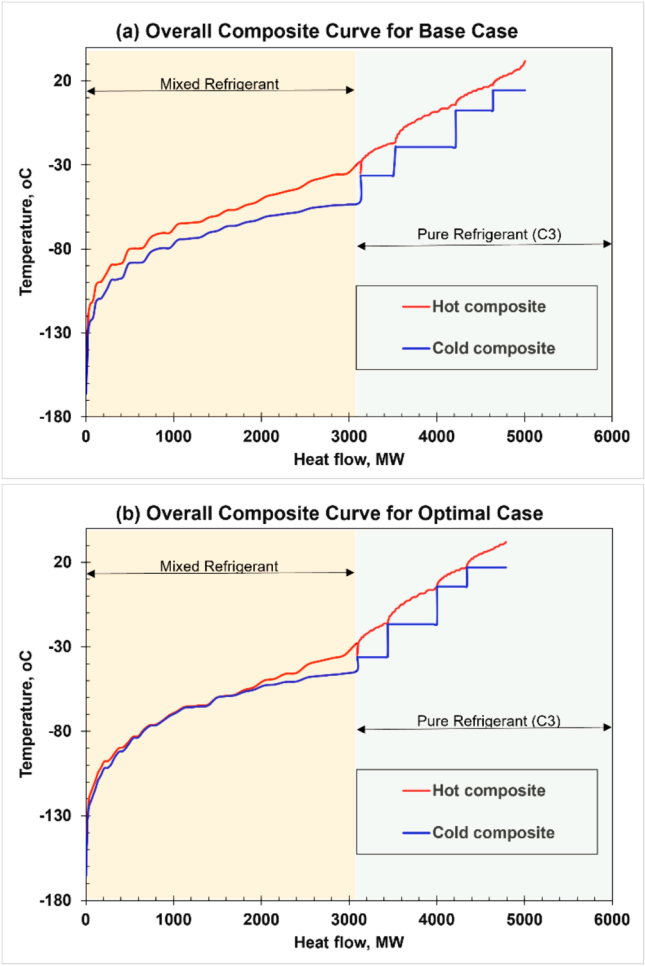

Fig. 10. Overall composition curve for (a) base case (b) optimal case.

4.2. *Optimized C3MR performance using constrained Bayesian optimization*

The CBO aimed to achieve the lowest possible SEC value using four refrigerant components – nitrogen, methane, ethane, and propane – at the lowest MR flow, with constant C3 flow and constant pressure values. The algorithm of CBO follows certain constraints to ensure a reliable SEC value without errors in the cycle. The code generated outputs that included the SEC value and the number of violated constraints. Fig. 12 illustrates on the horizontal axis, the number of violated constraints (out of 18 constraints) for each iteration with their frequency on the primary vertical axis. For example, looking at the green columns in Fig. 12, out of 1200 optimization iterations, around 450 iterations were violating 6 constraints and around 160 iterations were violating 2 constraints. As for the secondary vertical axis, it represents the trend of the SEC value in correlation with the number of violated constraints. The SEC value is lowest when a higher number of constraints are violated. However, as the code acts more strictly to specified constraints (moving left on the graph), the SEC value begins to increase. In the 0-constraint cluster, multiple SEC values were obtained, and the optimal one was approximately 0.268 kWh/kg_{LNG} at an MR flow of 301.08 kg/s and a constant C3 flow of 441.5 kg/s. This SEC value represents an improvement of around 13.6 % compared to the base case. The optimal mass fractions for the mixed refrigerant compositions at this optimal SEC value are (nitrogen: 0.0718, methane:0.2178, ethane: 0.2536, propane:0.4567).

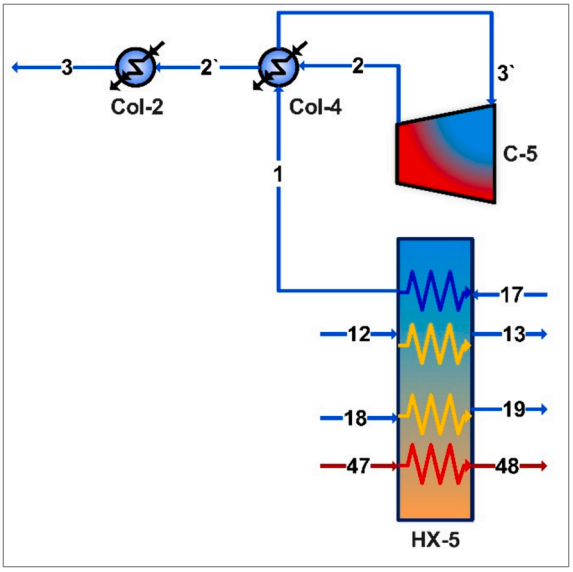

Fig. 11. Proposed schematic to recover the excessive cooling energy in stream 1.

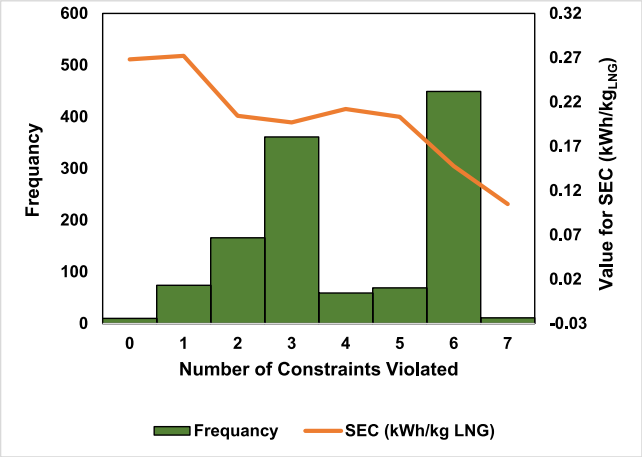

Fig. 12. Results of CBO iterations.

4.3. Comparison of the optimized C3MR performance using KBO and CBO

This section aims to compare the outcomes of both KBO and CBO methods and highlight their respective strengths and limitations. Firstly, concerning the objective function, assumptions, and constraints, both approaches are subjected to the same criteria. Secondly, both approaches utilized the identical cycle created in Aspen HYSYS V12, installed on the same PC to prevent roundoff errors. In terms of methodology, the KBO approach involved a three-step optimization process: initial optimization of the pressures and mass flow of the C3 loop, followed by the optimization of the pressures and mass flow of the MR loop and concluding with the optimization of the MR composition and mass flow. Conversely, the CBO approach relied on the results of step 2 from KBO as a baseline, initiating optimization of the MR composition and flow rate. Fig. 13 provides a summary of the results obtained from both approaches at each step. Analyzing the KBO results on the left side of the figure reveals that optimizing the MR loop led to a more significant improvement in the SEC value compared to the C3 loop, with the most significant contribution coming from modifying the MR composition. As for CBO, which showed a 7.3 % improvement over the base case, resulted in a 13.6 % reduction in the SEC value compared to the base case. In summary, both approaches yield SEC values that are significantly better than the base case by approximately 13–14 %.

The MR compositions achieved by both approaches are remarkably similar. The predominant component in the MR is propane, followed by ethane, methane, and nitrogen having the lowest proportion. This implies that approximately 46 % of the MR composition is allocated to the heavier hydrocarbons. This composition contributes to the low SEC values as the compressors experience a reduced load, requiring less power to compress the flow due to the presence of heavier hydrocarbons compared to the base case. Knowing that both approaches reach similar SEC values, each method has its own strengths and limitations. Regarding resource requirements, the KBO approach demands expertise in thermodynamics and mechanical aspects, while the CBO requires

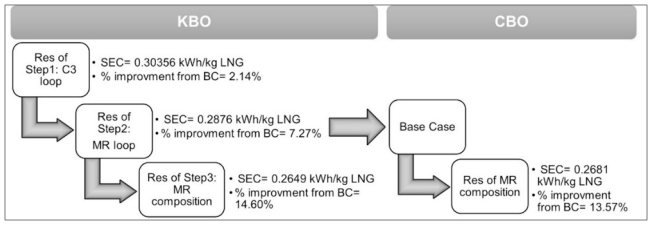

Fig. 13. Summary of SEC improvement at each optimization step.

coding proficiency, particularly in using the Bayesian optimization package with Python. In terms of exploration and exploitation, KBO relies on the knowledge and experience of the expert, whereas CBO explores a larger sample space within the constraints, accuracy limitations, and computational power of the PC. Regarding adaptability, the expert using KBO adjusts the simulation based on their experience and observations, while the CBO algorithm can adapt and improve through many iterations. Considering the speed of iterations, KBO is a slower approach since it is controlled by expert availability, whereas CBO is faster as it operates as an automated process. Thus, to optimize outcomes, we propose employing the KBO in steady-state conditions when plant operations are trouble-free, and there is sufficient time for cycle enhancement without urgency. Conversely, in dynamic conditions characterized by machine issues or a shortage of specific MR components, the recommendation is to utilize the CBO approach. This is attributed to its capacity to conduct numerous iterations quickly, and the accessibility it has to the control systems of the machine and the software, providing an alternative solution without human intervention.

4.4. Comparison with other optimization studies

As both KBO and CBO approaches reach a comparable SEC value, this section will rely on the SEC value optimized by KBO. This value will be compared with the base case, values reported in the literature for plants with similar capacity, and industrial SEC values as documented in some references.

4.4.1. Comparison with the base case

In this subsection, the optimal case obtained by KBO will be compared with the base case, which shares the same capacity of 120 kg/s, mirroring the scale of the model developed in this study to represent a large-scale plant. The SEC value of the base case simulates the existing nominal conditions in the literature for the C3MR, and it also represents the typical range for SEC in the industry.

Table 10 highlights important parameters for comparing the performance of the C3MR liquefaction process between the base case and the optimal case determined by KBO. Both cases use the same components for the mix refrigerant (MR), including N2, CH4, C2H6, and C3H8. However, in the optimal case, there is an increased portion of heavyweight hydrocarbons such as C3H8, with a slight reduction in the flow rates of both MR and pure refrigerant compared to the base case (BC). The table provides insights into compressor power consumption, heat exchanger (HX) cooling duties, and cooler loads for both cases, which will be discussed in detail. Additionally, the table highlights improvements in the COP, SEC, and CO_2 emissions as performance indicators.

4.4.1.1. Compression power. In terms of compression power for both the base case (BC) and the optimal case, the latter recorded a reduction in compression power for the six compressors in the cycle, amounting to approximately 18 MW. This reduction is reflected in the SEC value, as SEC is primarily influenced by the compression power consumed by the compressors and the LNG flow, as per Eq. (1). Given that the LNG flow remains constant, and the compression power is reduced by 18 MW, the SEC value decreases from 0.3102 to 0.2649 kWh/kg LNG, representing an approximate 14 % improvement compared to the BC. Fig. 14 illustrates the distribution of the total compression power among the six compressors in both the BC and the optimal case. From the figure, it is observed that the distribution percentage has not changed significantly, with the MR compressors consuming approximately 70 % of the total compression power. This highlights that, for future research opportunities, focusing on optimizing the MR loop will likely have a more substantial impact on the C3MR cycle performance than optimizing the C3 loop. Nevertheless, in terms of megawatts (MW), the power consumption by the MR compressors is reduced, as highlighted in Table 10.

Internal calculations demonstrate the 14 % reduction in the SEC

Table 10
C3MR process optimization results.

Parameters	Base case	Optimum case by KBO
Feed natural gas flow, (kg/h)	120	120
LNG flow, (kg/s)	110.6	110.6
Flash gas flow, (kg/s)	9.36	9.36
C3 flow rate (kg/s)	446	441.5 ↓
MR flow rate (kg/s)	300	294 ↓
MR Composition	N2: 0.0725 CH4: 0.2480 C2H6: 0.3323C3H8: 0.3472	N2: 0.0625 CH4: 0.2230 C2H6: 0.2473C3H8: 0.4672
Power of C-1, (MW)	2.460	2.581
Power of C-2, (MW)	8.782	8.031
Power of C-3, (MW)	6.584	5.504
Power of C-4, (MW)	20.08	16.98
Power of C-5, (MW)	56.44	45.75
Power of C-6, (MW)	29.20	26.67
$\sum_1^6 \dot{W}_{Comp.n}$**(MW)**	**123.6**	**105.5** ↓
Specific power, (kWh/kg LNG)	**0.3102**	**0.2649** ↓
Cooling duty of HX-1, (MW)	23.13	32.47
Cooling duty of HX-2, (MW)	27.01	23.69
Cooling duty of HX-3, (MW)	43.40	38.46
Cooling duty of HX-4, (MW)	23.90	21.89
Cooling duty of HX-5, (MW)	148.95	147.0
Cooling duty of HX-6, (MW)	18.00	16.18
$\sum_1^6 Q_{HX.n}$**(MW)**	**284.4**	**279.7**↓
$Q_{minimum}$(MW)	92.28	92.28
$Q_{internal}$(MW)	192.20	187.42 ↓
$COP_{Overall}$	**2.30**	
$COP_{indicative}$	**0.75**	**0.875** ↑
Cooler Load of Q_AC-1, (MW)	155.35	149.62
Cooler Load of Q_AC-2, (MW)	44.32	47.61
Cooler Load of Q_AC-3, (MW)	16.25	0.659
$\sum_1^3 Q_{Cooler.n}$**(MW)**	**216**	**198** ↓
$CO2_{emissions}$**(tons/year)**	**48,247**	**41,203** ↓
Economic results of operational costs		
Liquefaction capacity, (tons per day)	10,000	10,000
Utilization factor, (%)	85	85
Number of trains	14	14
Operational costs (million $/year)	497.04	424.45
Cost savings million $/year, (at an electricity price of 3.50¢/kWh)	0	72.59

value, as achieved in this study, holds significant consequences when translated into potential cost savings. In particular, the optimized case saves about 0.042 kWh/kg_{LNG}, which is equivalent for 4.77 million $/year for each C3MR train at an electricity price of 3.50 ¢/kWh. Thus, tacking QatarEnergy-LNG as an example, which possesses 14 AP-C3MR^{TM} cycles operating 14 LNG trains as mentioned in (Air Products), the amount of savings if the proposed optimal case of this study is applied, will be around 72.59 million $/yr.

An important note to add is that the reduction in compression power, leading to substantial cost savings, will benefit both existing systems operated by the C3MR process and future systems. This reduction will lower operational costs for current systems and decrease both the capital and operational costs for future systems. Furthermore, since AP-C3MR^{TM} acts as the foundation for the AP-X LNG process, the optimized case can also yield savings for the AP-X process.

4.4.1.2. HX's cooling duty. Regarding the cooling duty of the heat exchangers, a comparison between the base case (BC) and the optimal case indicates a decrease in the total cooling duty for the six heat exchangers from 284.4 MW to 279.7 MW. Consequently, a more compact size for the HXs becomes adequate to accomplish the same load of the base case. This improvement is useful for existing C3MR cycles equipped with modular HXs, allowing for the separation of some modules to be utilized in more useful applications. Additionally, this improvement holds value for future systems, as it requires a smaller HX size, thereby reducing space requirements.

4.4.1.3. Coolers load. In terms of coolers load, there are 3 coolers in the C3MR cycle which are responsible for cooling the flow at the outlets of the process compressors. Table 10, presents $\sum_1^3 Q_{Cooler.n}$ in MW for the base case and the optimal case by the KBO approach. It is noticed that the total coolers' load for the optimal cycle is lower than the base case by around 8.3 %. This decrease indicates that less power consumption is required by the coolers of the optimized case to cool down the MR in the cycle if it is an air-cooled system. In addition, the optimized cycle will require, a reduced water flow rate and compression power consumed by pumps if the coolers depend on water as a cooling median. Such improvements are advantageous for both existing C3MR cycles and future cycles.

4.4.1.4. CO_2 emissions. Lastly, an essential consideration is the current importance of CO_2 emissions nowadays. These emissions can occur because of energy-intensive procedures, including the compression and cooling of natural gas, as well as from the flaring or combustion of by-products. Such emissions significantly contribute to climate change, requiring careful monitoring and concerted efforts to develop approaches aimed at their reduction. In this context, the optimal case successfully reduced CO_2 emissions from 48,247 to 41,201 tons per year, translating to a saving of approximately 7 tons of CO_2 emissions annually. To contextualize these numbers, a comparative analysis was conducted, comparing the optimized case, base case, and other liquefaction processes in terms of CO_2 emissions, as illustrated in Fig. 15. These values were computed based on the SEC values outlined in (Vatani et al., Feb. 2014), utilizing Equation (12) from (Sleiti et al., 2023). The CO_2 emission quantities, measured in tons per year, were calculated for each process, considering an NG flow of 120 kg/s, and assuming the machine operates throughout the entire year with a CO_2 emission rate of 0.0000411 tons/kWh (Sleiti et al., 2023). Fig. 15 reveals that the proposed optimized C3MR process in this study achieves a remarkable 17 %

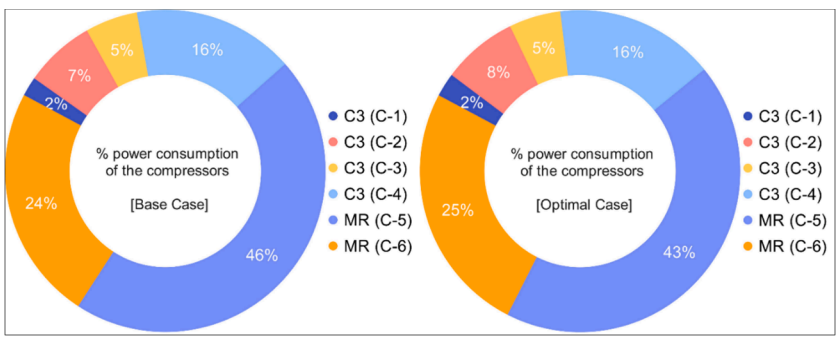

Fig. 14. Compressors power consumption percentage for BC and optimal case.

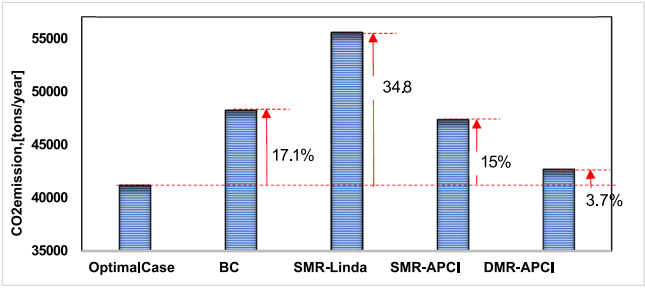

Fig. 15. CO_2 emissions for the optimal case, BC and other cryogenic processes.

reduction in CO_2 emissions compared to the base case and up to 35 % compared to four other technologies.

$$CO_{2emissions}\left[\frac{tons}{year}\right] = SEC\left[\frac{kWh}{kgLNG}\right] \times \dot{m}_{NG}\left[\frac{kg}{h}\right] \times CO_{2emissions}\left[\frac{tons}{kWh}\right] \times 8760\left[\frac{h}{year}\right] \quad (12)$$

4.4.2. Comparison with the literature

Table 11 displays two papers from open literature that share the same capacity as the present study and focus on optimizing the performance of the C3MR process. We obtained the optimal SEC (using the proposed approach in this study) under the same optimization conditions and simulation setting of these studies (see Appendix A, Table A1). Examining the table reveals that the optimized case demonstrates a percentage improvement ranging from 14.5 % to 38.6 % when compared to (Wang et al., 2013), and (Furda et al., 2022). This confirms the robustness of the proposed approach to identify the optimal performance of the process under different gas compositions and operating conditions.

4.4.3. Comparison with the industrial SEC

According to industrial values documented in (Alabdulkarem et al., 2011); (Sun et al., 2016), and (Furda et al., 2022), the percentage improvement of this study over the reported SEC ranges between 9 % and 30 %. This indicates that comparing the industrial values with the optimized case will demonstrate superior performance for the current study. Hence, we recommend considering the optimization of both existing and future LNG trains operating with C3MR using the proposed optimized case. This option has demonstrated greater efficiency, cost-effectiveness, and a smaller footprint compared to existing systems.

5. Conclusions

This study presents a comprehensive exploration of the propane pre-cooled mixed refrigerant (C3MR) process for natural gas liquefaction, aiming at performance optimization (minimizing energy consumption of the process). Two optimization approaches were performed in this study: Knowledge-based optimization (KBO) and constrained Bayesian optimization (CBO). Additionally, practical considerations for cycle components were taken into account. The key findings of this study are summarized as follows:

- The KBO approach successfully achieved a 14.6 % reduction in SEC compared to the base case. Similarly, the CBO approach reduced SEC by approximately 13.6 %, closely aligning with the KBO results.
- The proposed optimization approach in this study reduces the SEC by 14.5 % to 38.6 %. compared to the SEC of the C3MR in open literature.
- The SEC reduction to 0.264 kWh/kg_{LNG} is translated into an 18 MW decrease in compression power, yielding annual savings of 4.7 million $ per C3MR process with a capacity of 10,000 TPD.
- The coefficient of performance (COP) of the cryogenic cooling process recorded an improvement of approximately 15 % compared to the base case. This enhancement implies a reduction in the allocated area for the heat exchangers and a decrease in the internal cooling losses within the cycle.
- The optimization process reduced cooler duty, indicating lower power consumption for air-cooled systems and reduced water flow rates for pumps in case of water-cooled systems.
- CO_2 emissions decreased by 7 tons per year, representing a 17 % reduction when comparing the optimal case to the base case.

The results of these optimization approaches demonstrated the superior performance of the proposed optimal case against the base case (See Table 10), literature (Table 11), and industrial SEC (Table 12), consistently highlighting the efficiency and cost-effectiveness of the proposed optimization approach. Further economic and multi-objective optimization (reducing both energy consumption and capital and operational costs of LNG processes) following the presented approach in this study is recommended for future work. The outcomes provide tangible benefits for the existing and future energy-intensive LNG processes with enhanced efficiency, reduced environmental impact, and optimized resource utilization.

CRediT authorship contribution statement

Roba Shady: Writing – review & editing, Writing – original draft, Validation, Software, Investigation, Conceptualization. **Samer F. Ahmed:** Funding acquisition, Project administration, Resources, Supervision, Writing – review & editing. **Ahmad K. Sleiti:** Conceptualization, Formal analysis, Funding acquisition, Investigation, Project administration, Supervision, Writing – original draft, Writing – review & editing.

Declaration of Competing Interest

The authors declare that they have no known competing financial interests or personal relationships that could have appeared to influence the work reported in this paper.

The authors declare the following financial interests/personal

Table 12
Comparative summary with C3MR industrial values for SEC.

Ref.	SEC, kWh/kg_{LNG}	% Improvement in SEC
(Alabdulkarem et al., 2011)	0.344–0.375	22.94 %–29.36 %
(Sun et al., 2016)	0.321	17.38 %
(Furda et al., 2022)	0.292–0.381	9.18 %–30.40 %

Table 11
Comparative summary of related studies.

Ref.	Optimization technique	Capacity, TBD	Ref. SEC, kWh/kg_{LNG}	SEC in this study, kWh/kg_{LNG}	% Improvement in SEC
(Wang et al., 2013)	Sequential search	8219	0.408	0.2506	38.58
(Furda et al., 2022)	GA, NSGA-II	9590	0.31	0.2651	14.48

* This negative value will be justified below.

relationships which may be considered as potential competing interests.

Data availability

Data will be made available on request.

Acknowledgments

The authors would like to thank Qatar University for its support. Open Access funding provided by the Qatar National Library.

Appendix A

Table A1
The optimal SEC of the C3MR process obtained in this study unser the same conditions and simulation setting in references (Wang et al., 2013) and (Furda et al., 2022).

Ref.	Key setting parameters						NG composition (Methane/Ethane/Propane/Butane/Nitrogen)	EOS	Optimal SEC in this study (kWh/kg_{LNG})
	ACT, (^oC)	η_c, (%)	T_{NG}, (^oC)	T_{LNG}, (^oC)	P_{NG}, (bar)	P_{LNG}, (bar)			
(Wang et al., 2013)	30	75	25	−161	50	1.01	(96.92, 2.94, 0.06, 0.01, 0.07), mole fraction %	PR	0.2506
(Furda et al., 2022)	35	78, 75	27	−160	65	1.01	(87.5, 5.5, 2.1, 0.5, 0.3, 4.1), mass fraction %	PR	0.2651

References

"Air Products' AP-X® LNG Technology and Equipment Selected for First Phase of Massive Expansion Project in Qatar.".

Alabdulkarem, A., Mortazavi, A., Hwang, Y., Radermacher, R., Rogers, P., 2011. Optimization of propane pre-cooled mixed refrigerant LNG plant. Appl. Therm. Eng. 31 (6–7), 1091–1098. https://doi.org/10.1016/j.applthermaleng.2010.12.003.

Al-Mutaz, I.S., Liu, X., Mazza, G., 2016. Natural gas liquefaction technologies - An overview. Oil Gas Eur. Mag. 42 (4), 213–218.

Bosma, P., Nagelvoort, R.K. (2009). "Liquefaction Technology; Developments through History," *Proc. 1st Annu. Gas Process. Symp.*, pp. 19–31, doi: 10.1016/B978-0-444-53292-3.50006-7.

Bozorgkhou, N., Pirouzfar, V., Su, C.H., 2022. Increasing the efficiency of liquefied natural gas production plant with considering appropriate refrigerant components. Environ. Prog. Sustain. Energy 41 (4), 1–11. https://doi.org/10.1002/ep.13806.

BP, "BP Energy Outlook 2017," 2017. https://www.bp.com/content/dam/bp/business-sites/en/global/corporate/pdfs/energyeconomics/energy-outlook/bp-energy-outlook-2017.pdf (accessed Nov. 24, 2023).

BP, "Methodological changes," 2023. https://www.bp.com/content/dam/bp/business-sites/en/global/corporate/pdfs/energyeconomics/statistical-review/bp-stats-review-2018-full-report.pdf (accessed Nov. 24, 2023).

Cao, Y., Mohammadian, M., Pirouzfar, V., Su, C.H., Khan, A., 2021. Break Even Point analysis of liquefied natural gas process and optimization of its refrigeration cycles with technical and economic considerations. Energy 237, 121643. https://doi.org/10.1016/j.energy.2021.121643.

Furda, P., Variny, M., Labovská, Z., 2022. Towards time-effective optimization: Enviro-economic study of the C3MR LNG process. Energy Convers. Manag. 260 (March) https://doi.org/10.1016/j.enconman.2022.115602.

Ghorbani, B., Hamedi, M.-H., Shirmohammadi, R., Hamedi, M., Mehrpooya, M., 2016. Exergoeconomic analysis and multi-objective Pareto optimization of the C3MR liquefaction process. Sustain. Energy Technol. Assessments 17, 56–67. https://doi.org/10.1016/j.seta.2016.09.001.

Hajji, A., Chahartaghi, M., Kahani, M., 2019. Thermodynamic analysis of natural gas liquefaction process with propane pre-cooled mixed refrigerant process (C3MR). Cryogenics (Guildf) 103. https://doi.org/10.1016/j.cryogenics.2019.102978.

He, T., Lin, W., 2020. A novel propane pre-cooled mixed refrigerant process for coproduction of LNG and high purity ethane. Energy 202. https://doi.org/10.1016/j.energy.2020.117784.

He, T., Lin, W., 2020. Energy saving research of natural gas liquefaction plant based on waste heat utilization of gas turbine exhaust. Energy Convers. Manag. 225 (September), 113468 https://doi.org/10.1016/j.enconman.2020.113468.

Husnil, Y.A., Park, C., Lee, M., Karimi, I.A., Srinivasan, R. (2012). *Simulation based Heuristics Approach for Plantwide Control of Propane Precooled Mixed Refrigerant in Natural Gas Liquefaction Process*, vol. 31, no. July. Elsevier Masson SAS, pp. 400–404. doi: 10.1016/B978-0-444-59507-2.50072-X.

"IGU World LNG Report 2015 Edition | IGU.".

Jin, C., Yuan, Y., Son, H., Lim, Y., 2022. Novel propane-free mixed refrigerant integrated with nitrogen expansion natural gas liquefaction process for offshore units. Energy 238, 121765. https://doi.org/10.1016/j.energy.2021.121765.

Katebah, M., Hussein, M., Al-musleh, E.I. (2020). *A Straightforward Optimization Approach for a Baseload Propane-Mixed Refrigerant Process*, vol. 48. doi: 10.1016/B978-0-12-823377-1.50321-9.

Khan, M.S., Lee, S., Rangaiah, G.P., Lee, M., 2013. Knowledge based decision making method for the selection of mixed refrigerant systems for energy efficient LNG processes. Appl. Energy 111, 1018–1031. https://doi.org/10.1016/j.apenergy.2013.06.010.

Khan, M.S., Karimi, I.A., Bahadori, A., Lee, M., 2015. Sequential coordinate random search for optimal operation of LNG (liquefied natural gas) plant. Energy 89, 757–767. https://doi.org/10.1016/j.energy.2015.06.021.

Khan, M.S., Karimi, I.A., Wood, D.A., Sep. 2017. Retrospective and future perspective of natural gas liquefaction and optimization technologies contributing to efficient LNG supply: a review. J. Nat. Gas Sci. Eng. 45, 165–188. https://doi.org/10.1016/J.JNGSE.2017.04.035.

Kumar, S., Kwon, H.T., Choi, K.H., Hyun Cho, J., Lim, W., Moon, I., 2011. Current status and future projections of LNG demand and supplies: a global prospective. Energy Policy 39 (7), 4097–4104. https://doi.org/10.1016/J.ENPOL.2011.03.067.

Lee, I., Tak, K., Lee, S., Ko, D., Moon, I., 2015. Decision making on liquefaction ratio for minimizing specific energy in a LNG pilot plant. Ind. Eng. Chem. Res. 54 (51), 12920–12927. https://doi.org/10.1021/acs.iecr.5b03687.

Lee, I., *et al.* (2012). *Optimization of Pure-Refrigerant Cycle Compressing Ratio on C3-MR Process*, vol. 31, no. July. Elsevier Masson SAS, pp. 1472–1476. doi: 10.1016/B978-0-444-59506-5.50125-5.

Lim, W., Choi, K., Moon, I., 2013. Current status and perspectives of Liquefied Natural Gas (LNG) plant design. Ind. Eng. Chem. Res. 52 (9), 3065–3088. https://doi.org/10.1021/IE302877G.

Mokhatab, S., Mak, J.Y., Valappil, J.V., Wood, D., 2013. Handbook of Liquefied Natural Gas. Gulf Professional Publishing.

Noh, W., Park, S., Kim, J., Lee, I., 2022. Comparative design, thermodynamic and techno-economic analysis of utilizing liquefied natural gas cold energy for hydrogen liquefaction processes. Int. J. Energy Res. 46 (9), 12926–12947. https://doi.org/10.1002/er.8064.

Park, J., Mun, H., Kim, J., Lee, I., 2022. Advanced natural gas liquefaction process on LNG supply chain with liquid air: from design to thermodynamic and techno-economic analyses. Energy Convers. Manag. 252 (September 2021), 115107 https://doi.org/10.1016/j.enconman.2021.115107.

Pereira, M.A.M., Santos, L.F., Caballero, J.A., Ravagnani, M.A.S.S., Costa, C.B.B., 2022. Energy and economic comparison of five mixed-refrigerant natural gas liquefaction processes. Energy Convers. Manag. 272 (May) https://doi.org/10.1016/j.enconman.2022.116364.

Primabudi, E., Morosuk, T., Tsatsaronis, G., 2019. Multi-objective optimization of propane pre-cooled mixed refrigerant (C3MR) LNG process. Energy 185, 492–504. https://doi.org/10.1016/j.energy.2019.07.035.

Qyyum, M.A., et al., 2020. Single-solution-based vortex search strategy for optimal design of offshore and onshore natural gas liquefaction processes. Energies 13 (7). https://doi.org/10.3390/en13071732.

Raeisdanaei, S., Pirouzfar, V., Su, C.H., 2022. Technical and economic assessment of processes for the LNG production in cycles with expander and refrigeration. Environ. Dev. Sustain. 24 (11), 13407–13425. https://doi.org/10.1007/s10668-021-02054-z.

Rao, H.N., Nair, S.K., Karimi, I.A., 2019. Operational optimization of processes with multistream heat exchangers using data-driven predictive modeling. Ind. Eng. Chem. Res 58, 22. https://doi.org/10.1021/acs.iecr.8b05270.

Rasmussen, C.E., Williams, C.K.I. (2006). *Gaussian Processes for Machine Learning*, vol. 7, no. 5. 2006. [Online]. Available: www.GaussianProcess.org/gpml.

Sabbagh, O., Fanaei, M.A., Arjomand, A., Ahmadi, M.H., 2021. Multi-objective optimization assessment of a new integrated scheme for co-production of natural gas liquids and liquefied natural gas. Sustain. Energy Technol. Assess. 47 https://doi.org/10.1016/j.seta.2021.101493.

Sanavandi, H., Ziabasharhagh, M., 2016. Design and comprehensive optimization of C3MR liquefaction natural gas cycle by considering operational constraints. J. Nat. Gas Sci. Eng. 29, 176–187. https://doi.org/10.1016/j.jngse.2015.12.055.

Santos, L.F., Costa, C.B.B., Caballero, J.A., Ravagnani, M.A.S.S., 2023. Multi-objective simulation–optimization via kriging surrogate models applied to natural gas liquefaction process design. Energy 262. https://doi.org/10.1016/j.energy.2022.125271.

Shayan, M., Pirouzfar, V., Sakhaeinia, H., 2020. Technological and economical analysis of flare recovery methods, and comparison of different steam and power generation systems. J. Therm. Anal. Calorim. 139 (4), 2399–2411. https://doi.org/10.1007/s10973-019-08429-9.

Sleiti, A.K., Al-Ammari, W.A., 2022. Systematic thermodynamic approach for designing mixed refrigerants used in hydrogen precooling process. Int. J. Hydrogen Energy 47 (48), 20915–20931. https://doi.org/10.1016/j.ijhydene.2022.04.233.

Sleiti, A.K., Al-Ammaria, W.A., Ghani, S., 2023. Novel dual-mixed refrigerant precooling process for high capacity hydrogen liquefaction plants with superior performance. J Energy Storage 66 (February), 107471. https://doi.org/10.1016/j.est.2023.107471.

Sleiti, A.K., Al-ammari, W.A., Ghani, S., Hussein, I.A., 2024. A novel hydrogen liquefaction process using dual mixed cryogenic refrigeration system: Energy, exergy, and economic analysis. Int. J. Hydrogen Energy 56 (September 2023), 1324–1339. https://doi.org/10.1016/j.ijhydene.2023.12.224.

Sleiti, A.K., Al-Ammari, W.A., 2023. Novel integration between propane pre-cooled mixed refrigerant LNG process and concentrated solar power system based on supercritical CO_2 power cycle. Energy Rep. 9, 4872–4892. https://doi.org/10.1016/j.egyr.2023.04.012.

Sleiti, A.K., Al-Ammaria, W.A., 2024. In: Design and Analysis of Liquid Hydrogen Technologies Liquefaction, Storage, and Distribution. Elsevier. https://doi.org/10.1016/B978-0-443-21438-7.00001-7.

Song, C., Tan, S., Qu, F., Liu, W., Wu, Y., 2019. Optimization of mixed refrigerant system for LNG processes through graphically reducing exergy destruction of cryogenic heat exchangers. Energy 168, 200–206. https://doi.org/10.1016/j.energy.2018.11.105.

Sun, H., Shu, D., Zhu, H. (2012). *Process optimization of one-stage propane pre-cooled MRC cycle for small-scale LNG plant*, vol. 516–517. 2012. doi: 10.4028/www.scientific.net/AMR.516-517.1184.

Sun, H., He Ding, D., He, M., Shoujun Sun, S., 2016. Simulation and optimisation of AP-X process in a large-scale LNG plant. J. Nat. Gas Sci. Eng. 32, 380–389. https://doi.org/10.1016/j.jngse.2016.04.039.

Sun, H., Geng, J., Na, F., Rong, G., Wang, C., 2022. Performance evaluation and comparison of commonly used optimization algorithms for natural gas liquefaction processes. Energy Rep. 8, 4787–4800. https://doi.org/10.1016/j.egyr.2022.03.164.

Vatani, A., Mehrpooya, M., Palizdar, A., 2014. Advanced exergetic analysis of five natural gas liquefaction processes. Energy Convers. Manag. 78, 720–737. https://doi.org/10.1016/J.ENCONMAN.2013.11.050.

Veldandi, P.K., Kurian, S., 2020. Design Optimization of C3MR Natural Gas Liquefaction Process. In: Computer Aided Chemical Engineering, vol. 48. Elsevier B.V, pp. 517–522. https://doi.org/10.1016/B978-0-12-823377-1.50087-2.

Wang, M., Zhang, J., Xu, Q., Li, K., 2011. Thermodynamic-analysis-based energy consumption minimization for natural gas liquefaction. Ind. Eng. Chem. Res. 50 (22), 12630–12640. https://doi.org/10.1021/ie2006388.

Wang, M., Zhang, J., Xu, Q., 2012. Optimal design and operation of a C3MR refrigeration system for natural gas liquefaction. Comput. Chem. Eng. 39, 84–95. https://doi.org/10.1016/j.compchemeng.2011.12.003.

Wang, M., Khalilpour, R., Abbas, A., 2013. Operation optimization of propane precooled mixed refrigerant processes. J. Nat. Gas Sci. Eng. 15, 93–105. https://doi.org/10.1016/j.jngse.2013.09.007.

Wang, M., Khalilpour, R., Abbas, A., 2014. Thermodynamic and economic optimization of LNG mixed refrigerant processes. Energy Convers. Manag. 88, 947–961. https://doi.org/10.1016/j.enconman.2014.09.007.

Xu, H., Song, Y., Zhang, Y., Song, H., 2022. Organic solid waste upgrading under natural gas for valuable liquid products formation: pilot demonstration of a highly integrated catalytic process. Bioresour. Technol. 346 (December 2021), 126645 https://doi.org/10.1016/j.biortech.2021.126645.

Yang, W.Y., Cao, W., Chung, T.S., Morris, J. (2005). *Applied Numerical Methods Using MATLAB®*. doi: 10.1002/0471705195.

Zhang, J., Meerman, H., Benders, R., Faaij, A., 2020. Comprehensive review of current natural gas liquefaction processes on technical and economic performance. Appl. Therm. Eng. 166, 114736 https://doi.org/10.1016/J.APPLTHERMALENG.2019.114736.